PHYSICAL REVIEW D **85,** 114504 (2012)

Two-color QCD with staggered fermions at finite temperature under the influence of a magnetic field

E.-M. Ilgenfritz,[1,2] M. Kalinowski,[2] M. Müller-Preussker,[2] B. Petersson,[2] and A. Schreiber[2]

[1]*Joint Institute for Nuclear Research, VBLHEP, 141980 Dubna, Russia*

[2]*Humboldt-Universität zu Berlin, Institut für Physik, 12489 Berlin, Germany*

(Received 28 March 2012; published 7 June 2012)

In this paper we investigate the influence of a constant external magnetic field on the finite-temperature phase structure and the chiral properties of a simplified lattice model for QCD. We assume an $SU(2)$ gauge symmetry and employ dynamical staggered fermions of identical mass without rooting, corresponding to $N_f = 4$ flavors of identical electric charge. For fixed mass (given in lattice units) the critical temperature is seen to rise with the magnetic field strength. For three fixed β values, selected such that we stay (i) within the chirally broken phase, (ii) within the transition region, or (iii) within the chirally restored phase, we study the approach to the chiral limit for various values of the magnetic field. Within the chirally broken (confinement) phase the chiral condensate is found to increase monotonically with a growing magnetic field strength. In the chiral limit the increase starts linear in agreement with a chiral model studied by Shushpanov and Smilga. Within the chirally restored (deconfinement) phase the chiral condensate tends to zero in the chiral limit, irrespective of the strength of the magnetic field.

DOI: 10.1103/PhysRevD.85.114504 PACS numbers: 11.15.Ha, 12.38.Aw, 12.38.Gc

I. INTRODUCTION

It is commonly believed that hadronic matter at high temperature undergoes a phase transition into another phase, traditionally called the ''quark-gluon plasma.'' Actually, *ab initio* numerical lattice simulations have shown that the high temperature behavior of QCD at low baryon number density is governed by two interrelated crossover phenomena, namely, the transition from a low temperature confined regime to a high temperature deconfined regime and the transition from a low temperature regime with spontaneously broken chiral symmetry to a high temperature regime with restored chiral symmetry. For a recent review see [1]. The behavior at large baryon densities, on the other hand, is only predicted by models, because in this case the lattice action is not real-valued in real QCD, which makes *ab initio* numerical simulations impossible. There are special model theories, however, where there is no sign problem at finite baryon density. This is the case, e.g., for $SU(2)$ gauge theory with dynamical fermions.

A very interesting question is how a strong external magnetic field modifies the properties of strong interactions at high temperature. Cosmological models suggest that very strong magnetic fields ($\sqrt{eB} \sim$ 1–2 GeV) have been produced at the electroweak phase transition [2]. Strong external magnetic fields cannot be ignored in noncentral heavy ion collisions at high energy, which are produced by the electric currents of the throughgoing spectator nucleons. Estimates of these fields range from $\sqrt{eB} \sim 100$ MeV for collisions at the Relativistic Heavy Ion Collider (RHIC) to $\sqrt{eB} \sim 500$ MeV at the LHC [3,4].

One spectacular consequence in noncentral heavy ion collisions is the so-called chiral magnetic effect, which was proposed in Ref. [3]. In the presence of a winding number transition in the strongly interacting [color $SU(3)$] gauge field, the magnetic field can induce a parallel electric current. This leads to event-by-event fluctuations of the electric charge asymmetry of emitted hadrons with respect to the reaction plane. Such charge fluctuations have, in fact, been seen in the STAR experiment at RHIC [5,6] and in the ALICE experiment at the LHC [7]. Whether these charge fluctuations actually come from the mechanism mentioned above is still under debate [8–10].

In the confinement region, the presence of an external constant magnetic field is expected to enhance the chiral symmetry breaking, i.e., to lead to an increase of the chiral condensate. This has been predicted in the Nambu-Jona-Lasinio model, as well as in the chiral model. Quantitatively, the growth of the chiral condensate with the magnetic field strength differs between the two approaches: in the NJL model the increase is predicted to be quadratic [11–13], while in the chiral model it is predicted to be linear in the chiral limit, for not too strong magnetic fields [14]. The latter result is due to the infrared divergences occurring order by order in the magnetic field in the limit when the pion mass goes to zero. In the full solution [15] the divergence disappears, because the magnetic field itself acts as an infrared regulator.

According to several model calculations for the finite-temperature transition, the presence of an external magnetic field leads to an increase of the transition temperature [16,17]. The effect of an external electric field has been studied within holographic studies only [17]. In a two-phase treatment of the chiral model [18,19] the temperature of the chiral phase transition is seen to decrease with increasing magnetic field, while the originally first order transition (suggested by a bag model) ends with vanishing

latent heat, becoming a crossover. The possibility of a different effect of a magnetic field on the chiral symmetry restoring transition on one hand (strongly increasing transition temperature) and on the deconfining transition on the other (moderately increasing transition temperature) has been pointed out in Ref. [20]. In the framework of a quark-meson model coupled to the Polyakov loop, the common crossover without magnetic field is seen to split into separate phase transitions.

In the chiral limit, above the transition one expects the chiral order parameter to vanish. In Ref. [14] it is shown with the help of Dyson-Schwinger equations for zero temperature in an external constant magnetic field (which is parametrically much larger than the other scales in the problem) that a quark mass proportional to $\sqrt{|eB|}$ is dynamically generated. This leads to a finite chiral condensate proportional to $|eB|^{3/2}$. If these considerations can be applied to the high temperature phase, too, even in the chiral limit the phase transition would disappear in strong enough magnetic fields.

Recently several lattice simulations have been performed in gauge theories with fermions coupled to a constant external magnetic field.[1] The inclusion of the magnetic field does not lead to a sign problem for dynamical fermions. The pioneering work was performed in Refs. [22–25]. There the simulations were done in quenched $SU(2)$ gauge theory coupled to overlap fermions. The chiral condensate was found to increase linearly with the magnetic field strength in the chiral limit even in very strong magnetic fields $\sqrt{eB} \leq 3$ GeV, both at zero temperature and at $T = 0.82T_c$ slightly below the critical temperature T_c. A later investigation, still within quenched QCD, tends to favor an increase of the chiral condensate with the magnetic field strength with an effective power 1.6 (2) [26]. Simulations in full QCD with two flavors using staggered fermions have been reported in Refs. [27,28]. The authors of these works find, in agreement with the earlier quenched simulations, that the chiral condensate grows with the magnetic field strength, but quadratically for not too large magnetic fields. They attribute this to their use of a finite quark mass, corresponding to a pion mass $m_\pi \approx 200$ MeV. They further find that the chiral condensate increases with the magnetic field in the whole range of finite temperatures, thus even in the transition region and beyond [27]. This, in turn, leads to an increase of the finite temperature transition temperature with the magnetic field strength. An opposite conclusion was very recently presented in [29], namely, that the transition temperature decreases with an increasing magnetic field strength. This comes about because the chiral condensate, although increasing in the confined region away from the transition, actually decreases with the magnetic field strength in the transition region. In this investigation the authors have performed the simulations using an improved action with $2 + 1$ flavors of dynamical staggered fermions. They suggest that their results (differing from others) are due to the fact that in their calculation the pion mass is lower, and the taste splitting considerably smaller. Both calculations use the "fourth root trick" for a single flavor in order to represent the right number of (nondegenerate) flavors.

In this article we investigate the case of $SU(2)$ gauge theory with dynamical fermions at finite temperature. The influence of the constant magnetic field should to a large extent depend on the chiral properties, as proposed in Ref. [14]. These are quite similar to those of QCD, even if the color group is different. Furthermore, in the $SU(2)$ theory one can extend the investigation to finite chemical potential, as well as study in detail the topological excitations, which should be responsible for the chiral magnetic effect. In this paper we still confine our interest to the response of the chiral condensate and the finite-temperature transition to the magnetic field.

We simulate the theory on the lattice, using staggered fermions, without invoking the root of the fermion determinant. In the continuum limit this leads to a four-flavor theory with equal electric charge, but we avoid the bias due to rooting. We can determine the influence of the unquenching by comparing with the simulations in quenched $SU(2)$ theory in Refs. [22–25]. We can, of course, also test the validity for this case of the models mentioned above.

In Sec. II we define the action and the order parameters. In Sec. III we describe the setup of our simulations and how we determine the scale by calculating the heavy quark potential and the pion mass at zero temperature. Section IV presents the results at finite temperature and with the magnetic field for the chiral condensate, the Polyakov loop, and the mean values of plaquettes differently oriented with respect to the magnetic field. Section V contains the conclusions.

II. SPECIFICATION OF THE ACTION AND DEFINITION OF THE ORDER PARAMETERS

To describe the finite-temperature theory we introduce a lattice of size $N_\tau \times N_\sigma^3$. The sites are enumerated by $n = (n_1, n_2, n_3, n_4)$, where the n_i are integers, $n_i = 1, 2, \ldots, N_\sigma$ for $i = 1, 2, 3$ and $n_4 = 1, 2, \ldots, N_\tau$. The fourth direction is the (inverse) temperature or (Euclidean) time direction. The lattice spacing is denoted by a. On the links $n \rightarrow n + \hat{\mu}$ we define group elements $U_\mu(n) \in SU(2)$, where $\mu = 1, 2, 3, 4$. For the gauge action we adopt the usual Wilson plaquette action

$$S_G = \frac{\beta}{2} \sum_n \sum_{\mu<\nu} \mathrm{tr}(1 - U_{\mu\nu}(n)), \qquad (1)$$

where $U_{\mu\nu}(n)$ is the $\mu\nu$ plaquette matrix attached to the site n:

[1] We emphasize that this task is conceptionally different from those where an external *color*-magnetic field acts additionally to the fluctuating color gauge field (see, e.g., [21] for a recent work).

$$U_{\mu\nu}(n) = U_\mu(n)U_\nu(n+\hat{\mu})U_\mu^\dagger(n+\hat{\nu})U_\nu^\dagger(n). \quad (2)$$

We want to introduce an external constant magnetic field to interact with the fermions. We therefore introduce electromagnetic potentials in the fermion action by new, commuting group elements on the links, namely, $V_\mu(n) = e^{i\theta_\mu(n)} \in U(1)$, with compact link angles $0 \le \theta_\mu(n) < 2\pi$. We further introduce staggered fermions as Grassmann variables $\bar{\psi}(n)$ and $\psi(n)$, which are color vectors in the fundamental representation of $SU(2)$. The fermionic part of the action becomes

$$S_F = a^3 \sum_{p,q} \bar{\psi}(p)[D(p,q) + ma\delta_{p,q}]\psi(q), \quad (3)$$

$$D(p,q) = \frac{1}{2}\sum_\mu \eta_\mu(p)[V_\mu(p)U_\mu(p)\delta_{p+\mu,q} - V_\mu^*(p-\mu)U_\mu^\dagger(p-\mu)\delta_{p-\mu,q}]. \quad (4)$$

The arguments p, q are integer four vectors denoting sites on the lattice and $\eta_\mu(p)$ are the usual staggered sign factors,

$$\eta_1(n) = 1, \quad (5)$$

$$\eta_\mu(n) = (-1)^{\sum_{\nu=1}^{\mu-1} n_\nu}, \qquad \mu = 2,3,4. \quad (6)$$

In Ref. [30] the authors propose a construction to include a constant magnetic field both in the continuum and on the lattice, with periodic boundary conditions in the spatial directions. In the continuum, to have a constant magnetic field $\vec{B} = (0,0,B)$ pointing in the z direction, they define the vector potentials as

$$A_\mu(x,y,z,t) = \frac{B}{2}(x\delta_{\mu,2} - y\delta_{\mu,1}). \quad (7)$$

Because of the periodic boundary conditions, delta functions are needed at the boundary. Then $\vec{B} = \mathbf{rot}\vec{A}$ is constant except on the boundary, where we obtain a large magnetic field, so that the average of the magnetic field is zero:

$$\frac{1}{L_x L_y}\int_{(x,y)\ \text{plane}} dxdyB_z = 0. \quad (8)$$

The translation of this construction to the lattice is a good choice, because the lattice sees the delta function only modulo 2π. A plaquette angle can be defined by

$$\theta_{\mu\nu}(n) = \Delta_\mu\theta_\nu - \Delta_\nu\theta_\mu, \quad (9)$$

where $\Delta_\nu f(n) \equiv (f(n+\nu) - f(n))/a$ is the lattice forward derivative acting on $\theta_\nu(n) \sim A_\nu(n)$. Then the electromagnetic plaquette part can be split as [31]

$$\theta_{\mu\nu} = [\theta]_{\mu\nu}(n) + 2\pi n_{\mu\nu}(n) \quad (10)$$

with $n_{\mu\nu}(n) = -2, -1, 0, 1, 2$. Plaquettes with $n_{\mu\nu} \neq 0$ are called Dirac plaquettes, and the reduced plaquette angle $[\theta]_{\mu\nu} \in [0, 2\pi)$ corresponds to the (gauge-invariant) electromagnetic flux through the plaquette.

A constant magnetic background field in the z direction penetrating all the (x,y) planes of finite size $N_\sigma \times N_\sigma$ with a constant magnetic flux ϕ per each (x,y) plaquette is realized by the following choice:

$$V_1(n) = e^{-i\phi n_2/2}(n_1 = 1,2,\ldots,N_\sigma - 1), \quad (11)$$

$$V_2(n) = e^{i\phi n_1/2}(n_2 = 1,2,\ldots,N_\sigma - 1), \quad (12)$$

$$V_1(N_\sigma, n_2, n_3, n_4) = e^{-i\phi(N_\sigma+1)n_2/2}, \quad (13)$$

$$V_2(n_1, N_\sigma, n_3, n_4) = e^{i\phi(N_\sigma+1)n_1/2}. \quad (14)$$

In order to have a constant flux also on the boundary it has to be quantized as follows (q denoting the same electric charge of all fermion flavors).

$$\phi \equiv a^2 qB = \frac{2\pi N_b}{N_\sigma^2}, \qquad N_b \in \mathbf{Z}. \quad (15)$$

Thus, on the lattice there is always a minimal nonvanishing flux. Because the angle is periodic, there is also a maximum flux. In fact one has to restrict oneself to $\phi \le \pi$, or $N_b \le N_\sigma^2/2$. At finite temperature this means that $\frac{\sqrt{qB}}{T}$ is restricted to the region

$$\sqrt{2\pi}\frac{N_\tau}{N_\sigma} \le \frac{\sqrt{qB}}{T} \le \sqrt{\pi}N_\tau. \quad (16)$$

In the case of color group $SU(2)$ there is a larger chiral symmetry than in color $SU(N)$ with $N > 2$, because the fundamental representation is equivalent to the conjugate one. In the continuum, for $B = m = 0$ there is a $U(2N_f)$ chiral symmetry, which is broken down to $Sp(2N_f)$ when the mass is different from zero. If the symmetry is spontaneously broken, there are $N_f(2N_f - 1) - 1$ Goldstone bosons, where the -1 (one less Goldstone boson) is due to the axial anomaly.

On the lattice, for $SU(N)$, $N > 2$ there is a global $U(1) \otimes U(1)$ chiral symmetry for $B = m = 0$. The nonsinglet axial symmetry is broken when $m \neq 0$. Lattice calculations show that it is also spontaneously broken, with one Goldstone boson. In color $SU(2)$ for $B = m = 0$ there is instead a global $U(2)$ chiral symmetry on the lattice. For $m \neq 0$, $B = 0$ it is broken down to $U(1)$. In the dynamical theory it is spontaneously broken giving rise to three Goldstone bosons. One of them is an electrically neutral meson, while the other two are a baryon and an antibaryon, which are electrically charged. Notice that in color $SU(2)$ the baryons are bosons. When $B \neq 0$ there is only one Goldstone meson. The baryons get masses proportional to $\sqrt{qB}$. The situation, as far as the Goldstone bosons are concerned, is thus quite similar to two-flavor QCD.

In order to study the influence of the external static magnetic field on the chiral condensate and on the phase structure, we measure the following (approximate) order parameters. The chiral condensate, which is an exact order parameter in the limit of vanishing quark mass, is given by

$$a^3\langle\bar{\psi}\psi\rangle = -\frac{1}{N_\tau N_\sigma^3}\frac{1}{4}\frac{\partial}{\partial(ma)}\log(Z) = \frac{1}{N_\tau N_\sigma^3}\frac{1}{4}\langle \mathrm{Tr}(D+ma)^{-1}\rangle, \quad (17)$$

where the partition function is

$$Z = \int \prod_{n,\mu} (d\bar{\psi}(n) d\psi(n) dU_\mu(n)) e^{-S_G - S_F}. \quad (18)$$

The factor $1/4$ is inserted because we define $\langle\bar{\psi}\psi\rangle$ per flavor, and our theory has 4 flavors.

In order to locate the phase transition we use the disconnected part of the susceptibility (later on called "chiral susceptibility" for simplicity),

$$\chi = \frac{1}{N_\tau N_\sigma^3}\frac{1}{4}\frac{\partial^2}{(\partial(ma))^2}\log(Z) = \chi_{\mathrm{conn}} + \chi_{\mathrm{disc}}, \quad (19)$$

$$\chi_{\mathrm{disc}} = \frac{1}{N_\tau N_\sigma^3}\frac{1}{16}(\langle(\mathrm{Tr}(D+ma)^{-1})^2\rangle - \langle \mathrm{Tr}(D+ma)^{-1}\rangle^2). \quad (20)$$

It is important to notice that these are bare quantities, which should be renormalized when comparing with continuum expectation values.

We further measure the average value of the order parameter for confinement, the Polyakov loop

$$\langle L\rangle = \frac{1}{N_\sigma^3}\sum_{n_1,n_2,n_3}\frac{1}{2}\left\langle \mathrm{Tr}\left(\prod_{n_4=1}^{N_\tau} U_4(n_1,n_2,n_3,n_4)\right)\right\rangle \quad (21)$$

and the corresponding susceptibility

$$\chi_L = N_\sigma^3(\langle L^2\rangle - \langle L\rangle^2). \quad (22)$$

Intuitively it is clear that a constant magnetic field oriented into one of the three space directions has to violate the three-dimensional isotropy of the system. The isotropy violation can only be caused by the coupling of the magnetic field to the fermionic part of the action and should become visible within the effective gauge action after the fermion degrees have been integrated out. In order to demonstrate this anisotropy one can easily compute the average non-Abelian plaquette values separately for the different space-time planes (μ,ν) (an averaging over the lattice is implied),

$$P_{\mu\nu} = \left\langle \frac{1}{2}\mathrm{Re}\,\mathrm{Tr}U_{\mu\nu}\right\rangle, \quad (23)$$

as a function of the magnetic field strength.

III. SETUP OF THE SIMULATIONS

In order to simulate the model with dynamical staggered fermions ($N_f = 4$) we employed the standard hybrid Monte Carlo algorithm. We chose the number of integration steps n_{int} and their "time" length $\delta\tau$ such that the length of a trajectory was $n_{\mathrm{int}}\delta\tau = 1$ while the acceptance rate was larger than 0.8. For the finite-temperature measurements we used a $16^3 \times 6$ lattice. We measured the chiral condensate on every fifth configuration, the Polyakov loop and the plaquette variables on every configuration. The chiral condensate was calculated with the random source method. Thereby we used 100 random sources per configuration. The integrated autocorrelation time was taken into account in all our error estimates. In general, apart from simulating very near to the transition temperature, the integrated autocorrelation times of all observables were estimated mostly well below 20. The number of configurations (trajectories) generated within a run varied between 1800 and 5000. In general, 300 configurations were discarded for initial thermalization.

We also made a scan of the susceptibilities χ_{disc} and χ_L near the transitions for different magnetic fields. For this aim we generated longer runs of length between 10^4 and 2×10^4 trajectories, while we measured the chiral condensate and the Polyakov loop with the usual frequency. The autocorrelation times were estimated to $O(25)$ near the transition points.

Some zero-temperature simulations on a lattice of size $16^3 \times 32$ without magnetic field were performed additionally in order to estimate the lattice spacing, the pion mass, and the critical temperature in physical units. We are, of course, aware of the fact that we are considering a fictitious world of two-color QCD with four flavors of identical electric charge q. Nevertheless, a scale determination provides a rough estimate how near we are to the chiral limit, and how large the explored magnetic field strengths are. The number of trajectories per β value used in the $T = 0$ case was 2000. Measurements were performed after every fourth trajectory.

At $T = 0$ we first calculated the pion propagator $C_\pi(t)$ for the three β values, 1.7, 1.8, and 1.9, fitting it to the usual form ($N_\tau = 32$)

TABLE I. Fit parameters in lattice units for the pion correlator $C_\pi(t)$ according to Eq. (24) and for the static potential $V_S(R)$ according to Eq. (26). The fit range for the pion correlator starts at lattice distance t_{min}.

		$C_\pi(t)$			$V_S(R)$			
β	t_{min}	C	$E = am_\pi$	χ^2_{dof}	A	B	σ	χ^2_{dof}
1.7	5	1.48(5)	0.265(1)	0.047	⋯	⋯	⋯	⋯
1.8	6	1.01(3)	0.285(1)	0.023	0.265(38)	0.370(42)	0.169(8)	0.872
1.9	8	0.311(11)	0.296(2)	0.039	0.265(9)	0.300(11)	0.0725(19)	0.681
2.1	⋯	⋯	⋯	⋯	0.250(9)	0.265(13)	0.0170(16)	1.93

$$C_\pi(t) = Ce^{-Et} + Ce^{E(t-N_\tau)}. \quad (24)$$

The fit parameters in lattice units can be found in Table I. Our results are compatible with earlier ones obtained for larger quark masses on smaller lattices [32].

Moreover, we computed the heavy quark potential from hypercubic-blocking-smeared (HYP-smeared) [33] Wilson loops (with HYP smearing in the version of Ref. [34]) and for comparison also with APE smearing [35] at the three β values 1.8, 1.9, and 2.1, by fitting it to the form

$$V(\vec{R}) = V_S(R) + C\left(\frac{1}{R} - G_L(\vec{R})\right) \quad (25)$$

with

$$V_S(R) = A - B/R + \sigma R, \quad (26)$$

where $G_L(\vec{R})$ is the free gluon propagator on the lattice. This correction is only important at short distances. For details of this procedure see [36]. The fit results obtained from the HYP-smeared data are presented in Table I, too.

In order to estimate the lattice spacing in physical units we have determined the Sommer scale parameter R_0 [37] related to the static force $F_S(R) \equiv dV_S/dR$ through the condition

$$F_S(R_0)R_0^2 = 1.65. \quad (27)$$

The values R_0/a found at $ma = 0.01$ for the three β values (1.8, 1.9, 2.1) are given in Table II. To get the scale in physical units, we adopted the physical value $r_0 = 0.468(4)$ fm fixed for QCD [38]. Our measurements of the scale a at the three β values are well fitted by the two-loop formula for the β function for the $SU(2)$ case and four flavors

$$a(\beta) = \frac{1}{\Lambda_L}\left(\frac{4\beta_0}{\beta}\right)^{(-\beta_1)/2\beta_0^2} \exp\left(\frac{-\beta}{8\beta_0}\right),$$
$$\beta_0 = \frac{7}{24}\pi^{-2}, \qquad \beta_1 = \frac{19}{384}\pi^{-4} \quad (28)$$

with $\Lambda_L = 0.006\,60(12)$ fm^{-1} and $\chi^2_{\rm dof} = 1.64$ (see Fig. 1). Thus, we used this formula for an extrapolation down to $\beta = 1.7$, where the lattice spacing a is too large to allow a safe determination of R_0. In this way we could roughly estimate the pion mass and the magnetic field strength also at this value of the bare coupling and $ma = 0.01$. In Table II we have collected all our results for setting the scale.

TABLE II. Results in physical units for the Sommer scale R_0, the lattice spacing a, the pion mass m_π, and the quantity $\sqrt{qB}$ characterizing the magnetic field strength for $N_b = 50$ flux units for various β values considered in Sec. IV. The values for $\beta = 1.7$ were estimated by extrapolating with the two-loop beta function.

β	R_0/a	a [fm]	m_π [MeV]	$\sqrt{qB_{N_b=50}}$ [GeV]
1.7	1.89(4)	0.248(4)	210(4)	0.881(15)
1.8	2.75(8)	0.170(5)	330(10)	1.29(4)
1.9	4.32(6)	0.108(2)	537(9)	2.02(3)
2.1	9.03(43)	0.052(2)	...	4.22(21)

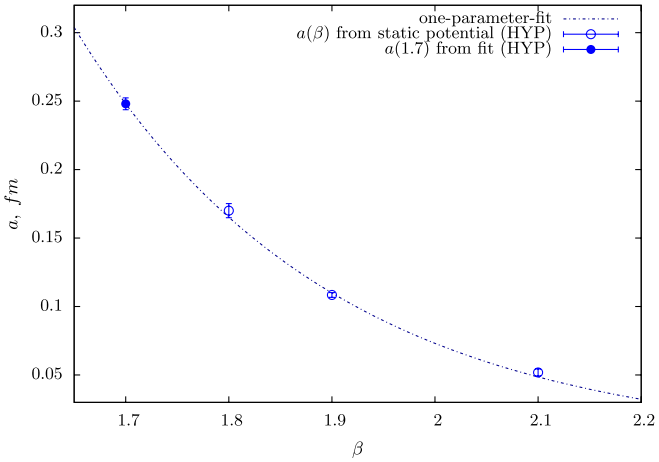

FIG. 1 (color online). The lattice spacing a vs β. The two-loop beta function according to Eq. (28) was used as a fit function, and $a(\beta = 1.7)$ was obtained through extrapolation.

Let us mention that for finite temperature with $N_\tau = 6$ and $ma = 0.01$ (for vanishing magnetic field strength) the critical value β_c will be seen close to $\beta = 1.8$. Thus, we are able to estimate also the critical temperature in physical units. We find $T_c \simeq 193(6)$ MeV.

IV. RESULTS AT FINITE TEMPERATURE

The finite-temperature simulations are performed on lattices of size $16^3 \times 6$. In Fig. 2 the bare chiral condensate is shown as a function of the flux number N_b for various values of β in the region of the transition value $\beta = \beta_c = 1.8$. Because the lattice is finite the chiral condensate is

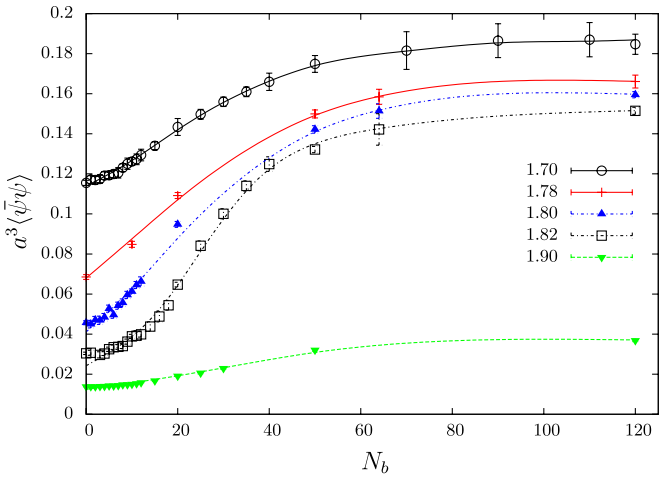

FIG. 2 (color online). The rising and saturation behavior of the chiral condensate as a function of the magnetic field in flux units for $am = 0.01$ and for various β values. The lattice size is $16^3 \times 6$. The curves are to guide the eyes.

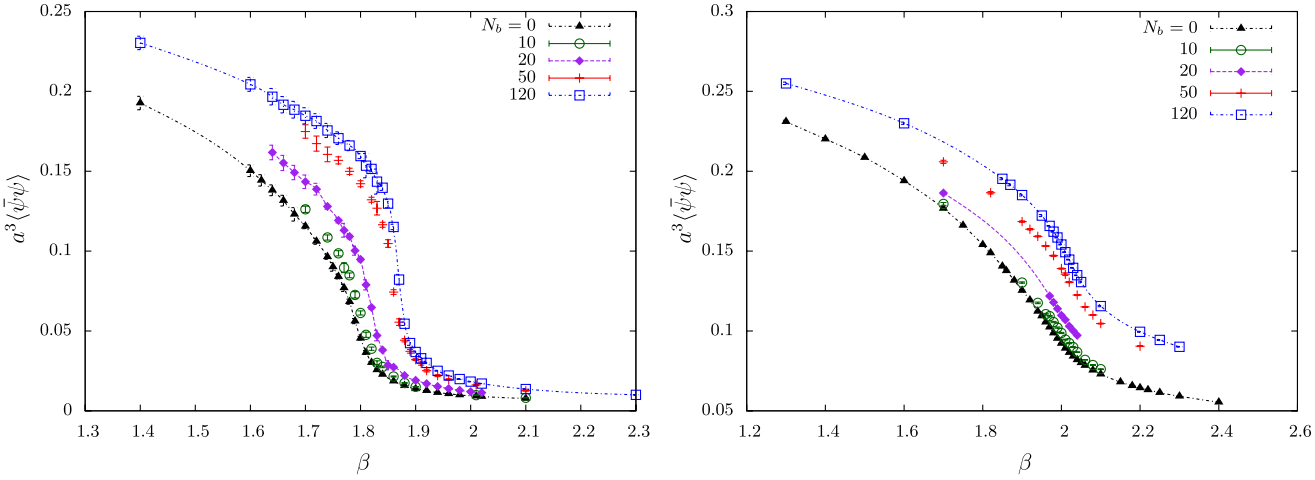

FIG. 3 (color online). The bare chiral condensate $a^3\langle\bar{\psi}\psi\rangle$ vs inverse coupling β for various magnetic fluxes ϕ (in flux units) and for two different bare masses $ma = 0.01$ (left panel) and $am = 0.1$ (right panel). The lattice size is $16^3 \times 6$. The curves are to guide the eyes.

periodic in the magnetic flux ϕ. We see that saturation effects set in at $N_b \approx 60$. This corresponds to $N_b \approx N_\sigma^2/4$ or $\phi \approx \pi/2$, which is half of the maximally achievable flux; see formula (16). Our investigation is mostly restricted to values of $N_b \leq 50$. The corresponding maximal values of $\sqrt{qB}$ are given in Table II. They are in general greater than the physical region of interest, $\sqrt{qB} \lesssim 1$ GeV. In Fig. 3 we plot the bare chiral condensate as a function of β for a set of numbers of flux quanta for the bare quark mass $ma = 0.01$ and 0.1. For the smaller quark mass we see quite clearly a transition for all values of the flux quanta N_b under consideration. It is important to notice that the bare chiral condensate increases with increasing magnetic field for fixed β, for all values of β in the transition region. This indicates that the chiral transition moves to higher temperatures as the magnetic field is increasing. This tendency is in agreement with the results in [27,28] but opposite to the tendency seen in [29] where the bare chiral condensate decreases with the flux ϕ in the transition region, leading to a decrease of the transition temperature. As shown in Sec. III, without the magnetic field, for $am = 0.01$ and close to T_c we have reached a ratio $m_\pi/T_c \approx 1.7$, which is similar to the ratio in [27,28], but higher than that in [29]. We also have a different gauge group. It is clear that our observation does not represent a direct contradiction to the results in [29].

For the higher quark mass $ma = 0.1$ the transition in the chiral condensate turns out very smoothly.

In Fig. 4 the expectation value of the Polyakov loop is shown vs β for the same two values of the bare quark mass. This is an indicator for the deconfinement transition. For the lower quark mass the deconfinement transition and the

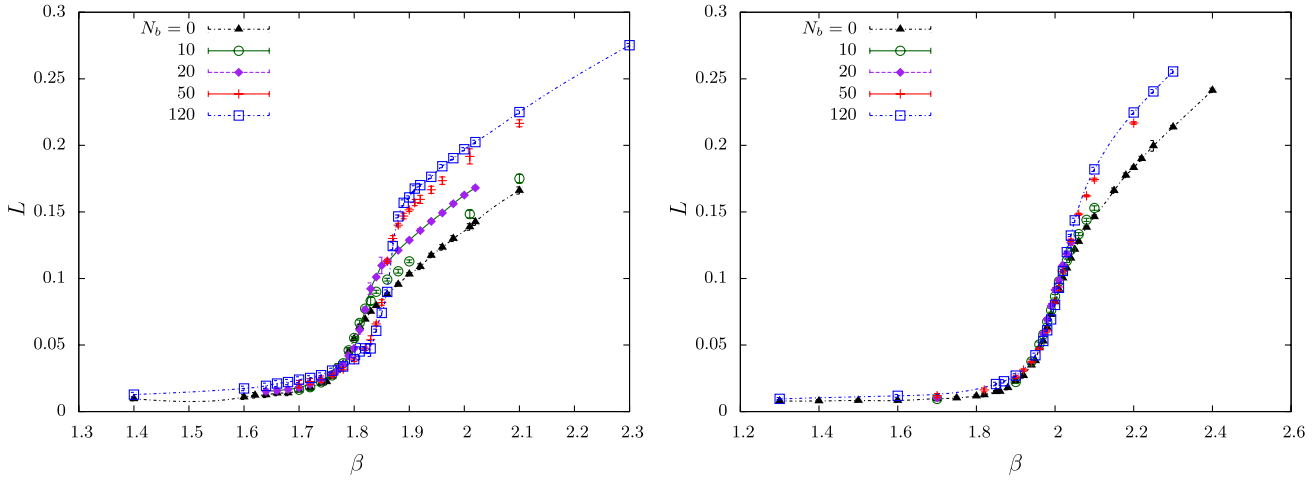

FIG. 4 (color online). The (unrenormalized) Polyakov loop expectation value $\langle L\rangle$ vs inverse coupling β for various magnetic fluxes ϕ and for two different bare masses $ma = 0.01$ (left panel) and $am = 0.1$ (right panel). The lattice size is $16^3 \times 6$. The curves are to guide the eyes.

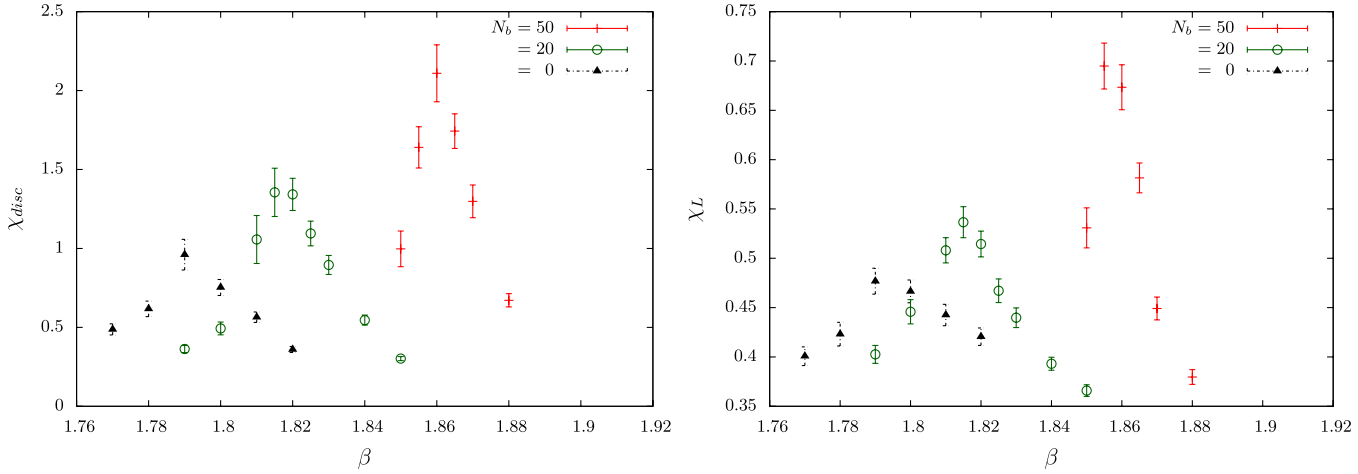

FIG. 5 (color online). The chiral susceptibility $\chi_{\rm disc}$ (left panel) and the Polyakov loop susceptibility χ_L (right panel), shown versus β at $am = 0.01$ for various magnetic fluxes corresponding to the lattice size $16^3 \times 6$ (see text). For the computation of $\chi_{\rm disc}$ 100 stochastic sources per configuration have been used.

chiral transition are consistent with happening at the same temperature. Furthermore, the transition temperature increases with the quark mass. At the high quark mass there seems to be only a weak effect of the magnetic field on the deconfinement temperature.

To study the change of the transition temperature at the lower quark mass more quantitatively we have calculated the susceptibilities. In Fig. 5 we show the chiral susceptibility and the Polyakov loop susceptibility for the low quark mass $ma = 0.01$. It is clearly seen in the left figure that the chiral transition indeed moves to higher temperatures as the magnetic field becomes stronger. In the right figure we show the same effect for the Polyakov loop susceptibility. In fact, the maxima of the two susceptibilities are at the same value for a given magnetic field. There is no sign of a splitting between the chiral and the deconfinement transition. The height of the peaks increases with the field strength. However, only a finite size scaling analysis could show if the transition remains a crossover or becomes a real phase transition.

In order to study the dependence of the chiral condensate on the magnetic field strength in the chiral limit, we have chosen to investigate in more detail the behavior of the chiral condensate as a function of the quark mass and the magnetic field for three fixed values of β. Because we keep β fixed as we vary the quark mass and the magnetic field, the lattice spacing a is also fixed and we have eliminated lattice effects coming from the variation of a. The three values are $\beta = 1.70$ (which is clearly in the confined phase), $\beta = 1.90$ (which is in the transition region), and

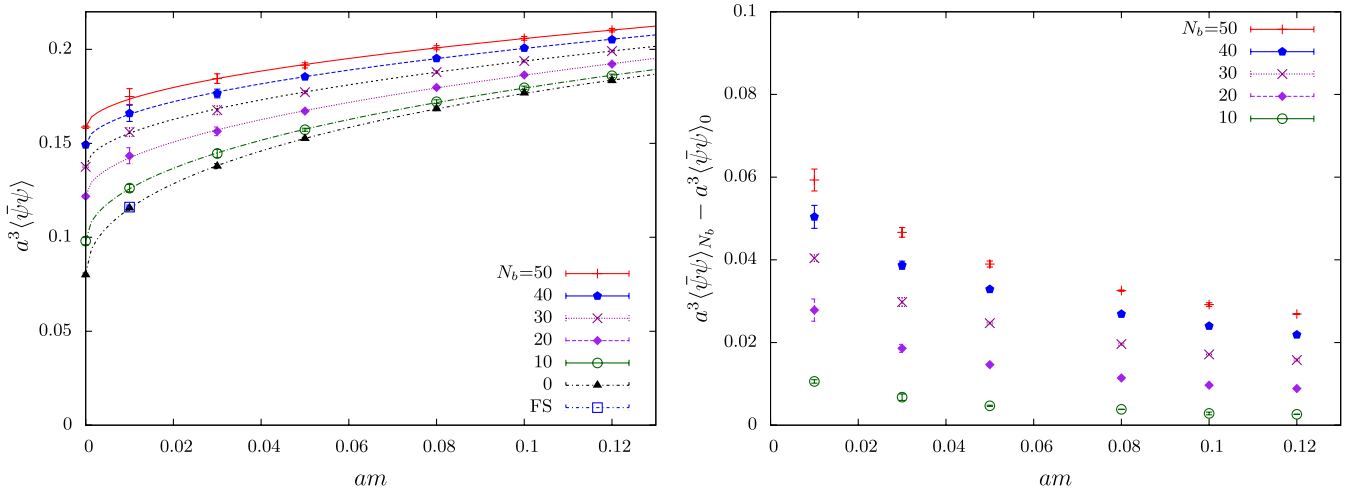

FIG. 6 (color online). Mass dependence of the bare chiral condensate (left) and of the subtracted chiral condensate (right) for various magnetic fluxes within the confinement phase ($\beta = 1.70$). The lattice size is $16^3 \times 6$. In order to check for the smallness of finite-size effects even for the lowest quark mass we show also a data point (FS) obtained with $24^3 \times 6$. The lines correspond to fits with the chiral fit function $f_1(ma)$ according to Table III.

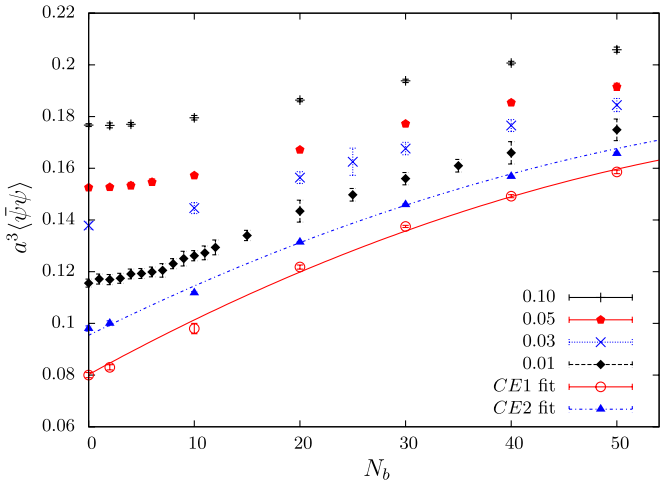

FIG. 7 (color online). The bare chiral condensate as a function of the flux for different masses and extrapolated to the chiral limit with f_1 according to Eq. (29) (circles) and f_2 according to Eq. (30) (triangles), respectively. The dotted lines show the corresponding chiral limit fit results CE1 and CE2 with the polynomial ansatz Eq. (31).

$\beta = 2.10$ (which is in the deconfined phase). Let us first discuss the results in the confined region.

In the left panel of Fig. 6 we show the dependence of the bare chiral condensate on the quark mass for various values of the magnetic flux. To obtain the results relevant to continuum physics, one has to subtract an additive divergence for finite quark mass, as well as do a multiplicative renormalization, which is needed also at zero mass. In the right panel of Fig. 6 we show the difference between the bare chiral condensate for finite fluxes subtracted by the same quantity at zero flux. This eliminates the main part of the additive divergence. In the left panel we have also included points at quark mass zero, where there are no additive divergencies. The values at zero quark mass are obtained by a chiral extrapolation. We perform this extrapolation in two ways. Because we are not very far from the transition, we suppose that we can use the formula for the reduced three-dimensional model [39]. See also [40–42]. In that case we may use the ansatz $a^3\langle\bar{\psi}\psi\rangle = f_1(ma)$, where

$$f_1(ma) = a_0 + a_1\sqrt{ma} + a_2 ma \tag{29}$$

with the nonanalytic term coming from the Goldstone bosons. Such a parametrization has been used in [38] in the context of the finite-temperature transition in QCD. As an alternative we also use the chiral extrapolation relevant for zero temperature, namely, $a^3\langle\bar{\psi}\psi\rangle = f_2(ma)$, where

$$f_2(ma) = b_0 + b_1 ma \log ma + b_2 ma. \tag{30}$$

The fits performed with Eq. (29) are shown as dashed or dotted lines in Fig. 7. The fit parameters of both kinds of fits are summarized for $\beta = 1.70$ and various magnetic fluxes in Table III.

The value of the bare chiral condensate in lattice units within the chiral limit ($m = 0$) for various values of the flux are given by a_0 and b_0, respectively. One can see that the statistical errors on the parameters are much smaller than the systematic errors coming from the fit formulas. We are, however, not interested in the absolute values of the bare chiral condensate at zero mass, but in the dependence of this value on the magnetic field strength. The flux dependent part does not need renormalization, and thus can be directly compared to continuum models. In Fig. 7 we show the bare chiral condensate as a function of the number of magnetic flux quanta for different bare quark masses. The chirally extrapolated points are obtained with the fit functions in Eqs. (29) and (30). One can see that for

TABLE IV. Fit parameters for the chiral condensate as a function of the magnetic flux N_b in the chiral limit according to the polynomial ansatz Eq. (31). CE1 and CE2 correspond to the chiral fit extrapolations with fit functions f_1 and f_2, respectively, as presented in Table III. Both the fit results are shown in Fig. 7.

	$g(N_b)$			
	c_0	c_1	c_2	$\chi^2_{\rm dof}$
CE1	0.080(1)	0.027(2)	−0.000 15(5)	1.18
CE2	0.095(2)	0.021(2)	−0.000 15(3)	9.4

TABLE III. Chiral fit parameters for the fits $f_1(ma)$ [Eq. (29)] and $f_2(ma)$ [Eq. (30)] allowing us to extrapolate to the chiral limit for $\beta = 1.70$ (chirally broken phase) and various magnetic field strengths. The fit curves obtained with f_1 are shown in the left panel of Fig. 6.

	$f_1(ma)$				$f_2(ma)$			
N_b	a_0	a_1	a_2	$\chi^2_{\rm dof}$	b_0	b_1	b_2	$\chi^2_{\rm dof}$
0	0.080(1)	0.36(1)	−0.19(2)	0.33	0.098(1)	−0.42(1)	−0.20(2)	0.73
2	0.083(1)	0.34(1)	−0.16(2)	0.20	0.100(1)	−0.42(1)	−0.16(3)	0.30
10	0.098(2)	0.28(1)	−0.09(3)	0.66	0.1118(5)	−0.28(1)	0.08(1)	0.10
20	0.1218(8)	0.203(3)	0	0.73	0.1314(2)	−0.238(1)	0	0.80
30	0.1375(4)	0.177(1)	0	0.20	0.1459(3)	−0.208(2)	0	0.18
40	0.1492(6)	0.162(2)	0	0.35	0.1568(2)	−0.1901(9)	0	0.05
50	0.1586(7)	0.149(2)	0	0.23	0.1657(5)	−0.174(2)	0	0.18

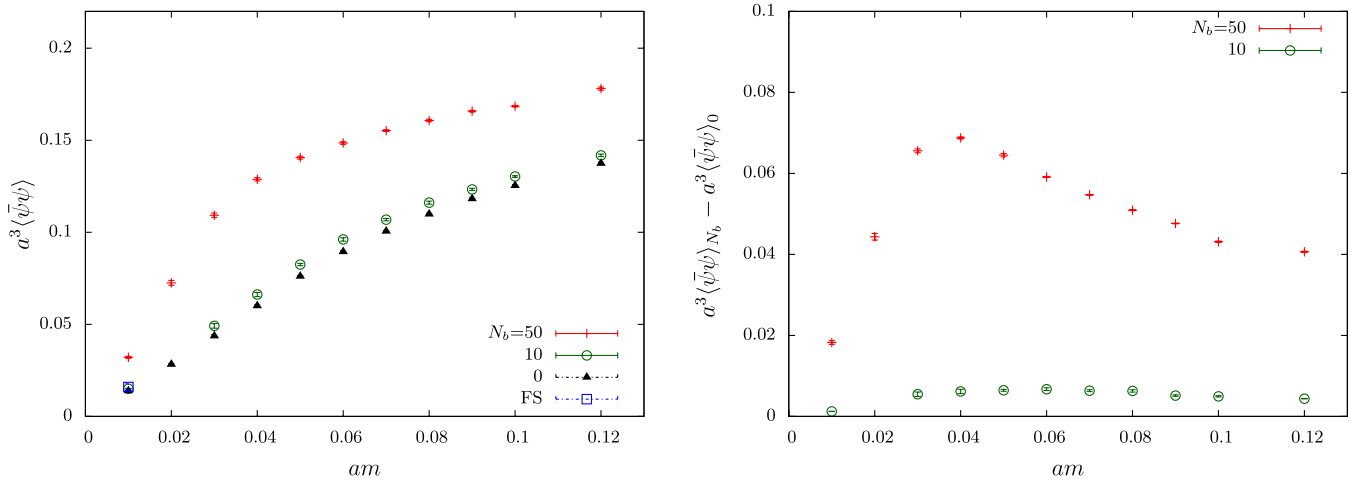

FIG. 8 (color online). Mass dependence of the bare chiral condensate (left) and of the subtracted chiral condensate (right) for three magnetic flux values within the transition region ($\beta = 1.90$). The lattice size is $16^3 \times 6$. For the lowest mass we show also a data point (FS) obtained with lattice size $24^3 \times 6$.

finite quark mass the data at small magnetic flux are consistent with a quadratic behavior, while the extrapolated values to $ma = 0$ seem to start with a linear behavior irrespective of the specific chiral extrapolation f_1 or f_2 used. This behavior is in agreement with the prediction of the chiral model of Ref. [14]. In Table IV we provide the fit parameters for the chiral condensate as a function of the magnetic flux $\phi \sim N_b$,

$$g(N_b) = c_0(1 + c_1 N_b + c_2 N_b^2), \tag{31}$$

in the chiral limit obtained with the chiral extrapolation f_1 (CE1) and f_2 (CE2), respectively. We have not calculated the pion decay constant, and therefore we do not make a quantitative comparison with the chiral model at finite temperature and magnetic field studied in Ref. [18].

Now we come to the transition region and the temperature region above the transition. In Fig. 8 we show the mass dependence of the bare chiral condensate (left panel) and the subtracted chiral condensate (right panel) in the transition region (at $\beta = 1.90$) for three values of the magnetic flux. One can see that for finite flux, as well as for zero flux, the bare and subtracted chiral condensates are consistent with extrapolating to zero in the chiral limit. For the highest flux, $N_b = 50$, one can clearly discern two regions of behavior. For $am \gtrsim 0.04$ the chiral condensate seems to extrapolate to a finite value, but for $am \lesssim 0.04$ it actually extrapolates to zero. This can be understood, if one assumes that the transition for $N_b = 50$ at this value of β takes place for $am \approx 0.04$. In Fig. 9 we present the same quantities as above, but for $\beta = 2.10$. This is well inside the chirally restored phase. The chiral condensate extrapolates to zero for all values of the flux. Thus chiral symmetry is restored for all values of the flux that we have investigated. Within our precision there is no evidence for a quark mass which is spontaneously created by the

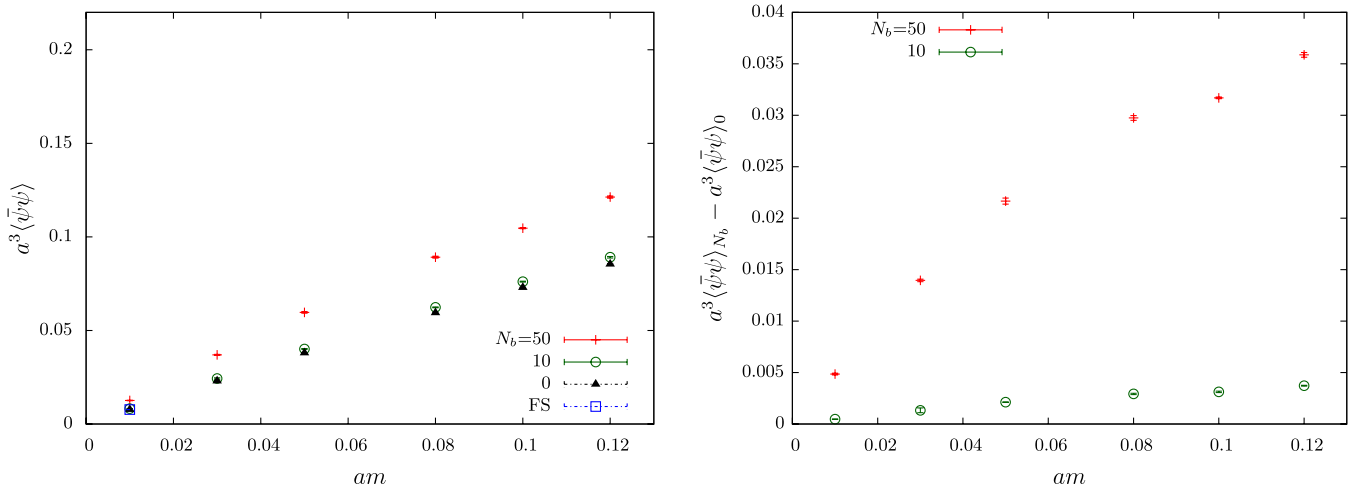

FIG. 9 (color online). Same as in Fig. 8 but within the deconfinement phase ($\beta = 2.1$).

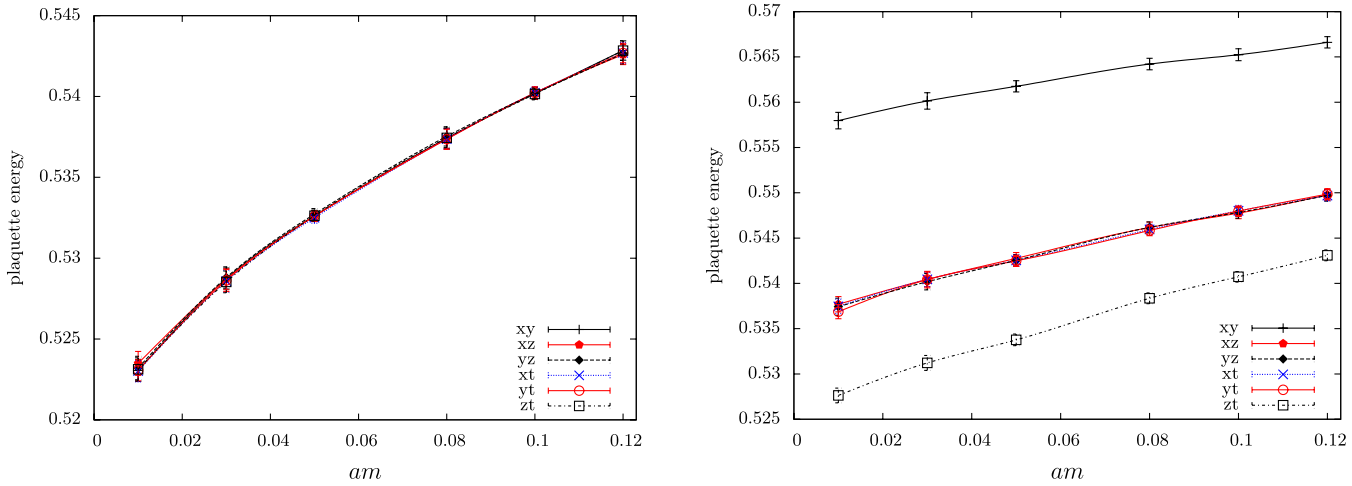

FIG. 10 (color online). Plaquette energies $(1 - P_{\mu\nu})$ in the confinement phase ($\beta = 1.70$) without (left) and with (right) an external magnetic field ($N_b = 50$). The curves are to guide the eyes.

magnetic field as suggested in a self-consistent calculation in [14] using the Dyson-Schwinger equations.

Finally, we study the indirect influence of the magnetic field on the gluonic part of the action. For this purpose we provide the plaquette energies $1 - P_{\mu\nu}$ individually for the six differently oriented plaquettes, as given in Eq. (23) for varying fermionic mass. We do this for the same values of β as above, namely, $\beta = 1.70$, 1.90, and 2.10 and for two values of the flux corresponding to $N_b = 0$ (zero magnetic field) and $N_b = 50$ (strong magnetic field).

In Fig. 10 one can see that at $\beta = 1.70$ (within the confined phase) all the plaquettes are degenerate for vanishing magnetic field. For a strong magnetic field pointing into the z direction, the xy and the zt plaquettes become well separated from the others. This effect can be qualitatively understood by representing the effective gauge action in terms of fermionic loops within a hopping parameter expansion for large fermion mass $am \sim 1/\kappa$. While in the order κ^4 of such an expansion only xy plaquettes receive a coupling to the magnetic field strength, in the order κ^6 loops extending into three directions xyz or xyt may couple to it. The zt plane is distinct, since only in the order κ^8 and beyond there exist loops extending into all four directions which couple to the magnetic field in the effective action.

In Fig. 11 the same plots are shown for $\beta = 1.90$ (in the transition region). For vanishing magnetic field now the spacelike and the timelike plaquettes are different from each other for sufficient small quark mass. This is the well-known temperature effect observed in the deconfined phase and providing a nonvanishing energy density (see, e.g., [43]). However, in the right panel one can see that, with a strong magnetic field applied, the splitting of the xy and the zt plaquettes from the others is even stronger than the splitting between the other spacelike and timelike plaquettes. Deep in the deconfined phase these results become even more pronounced—see Fig. 12.

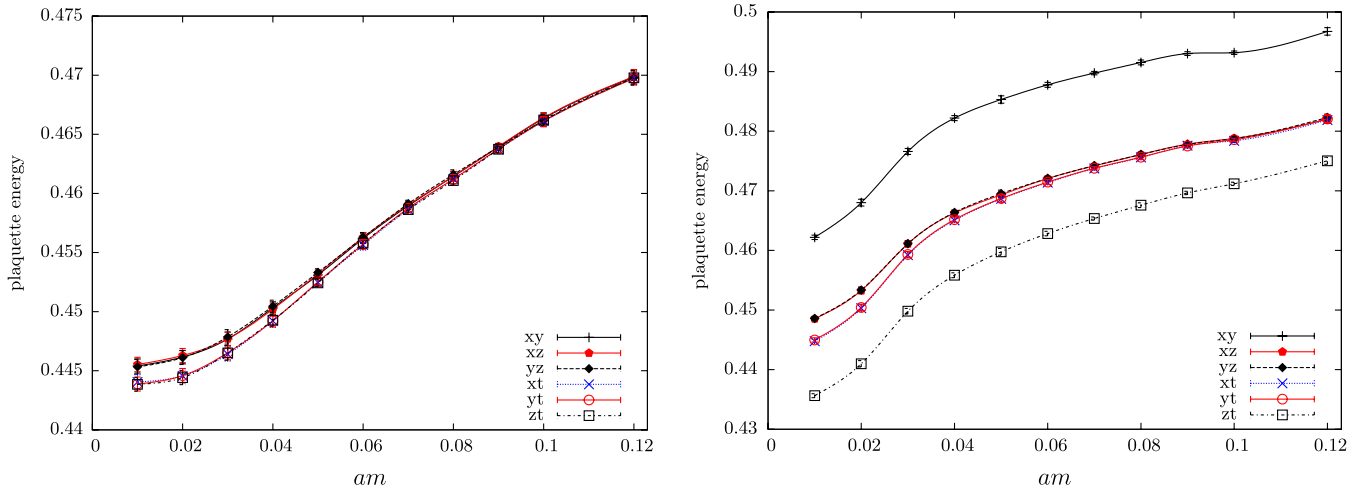

FIG. 11 (color online). Same as in Fig. 10 but for $\beta = 1.90$ (transition region).

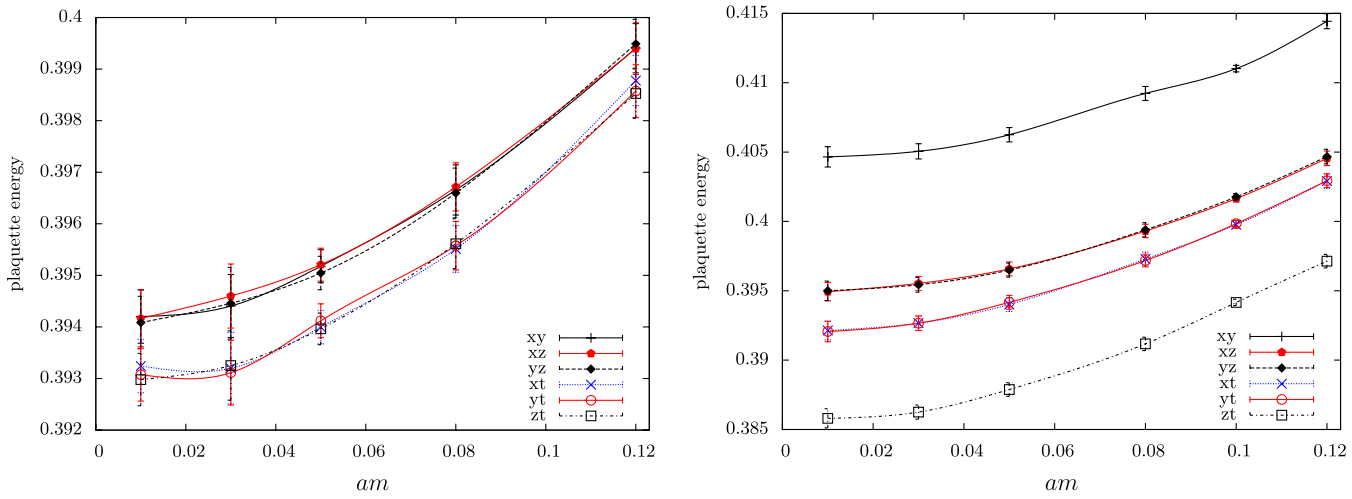

FIG. 12 (color online). Same as in Fig. 10 but for $\beta = 2.10$ (deconfinement phase).

V. CONCLUSIONS

We have investigated two-color QCD at finite temperature in an external magnetic field using lattice simulations. We have, in particular, studied how the magnetic field influences the chiral properties of the theory. As the chiral properties of this theory are similar to those of QCD, our results should be relevant also for the physical case.

We have found for all temperatures for fixed bare quark mass that the chiral condensate grows with the magnetic field. Hence, the temperature of the chiral phase transition grows with the strength of the magnetic field. This is confirmed by a measurement locating the peak of the chiral susceptibility. At the phase transition the pion mass is around 1.5 times the critical temperature. A similar result had been found by [27,28] in QCD with about the same ratio of the pion mass to the critical temperature. The opposite conclusion was reached in [29], claiming that the transition temperature decreases with the magnetic field in QCD with the physical pion mass. It would be interesting to see if the result in our model is valid in the chiral limit, but we leave this to a future investigation. Furthermore, we have shown, by measuring the susceptibility of the Polyakov loop, that the deconfinement and the chiral transitions move together to the same temperature, if small or large magnetic fields are switched on.

In this work, by extending our measurements to several values of the quark mass, we make a first investigation of the chiral limit of the theory at three values of the temperature, one in the confined region, one in the transition region, and another deep in the deconfined phase. In the chiral limit there is no additive renormalization necessary for the chiral condensate. In the confined region, we find that the chiral condensate in the chiral limit seems to grow linearly with the magnetic field strength. This is in agreement with the prediction of the chiral model at zero temperature.

At the other two values of the temperature chosen, the chiral condensate extrapolates to zero for all values of the magnetic field. Thus, in the chiral limit there is a real chiral phase transition, which does not disappear for strong magnetic fields.

We have also investigated the influence of the magnetic field on the gluonic part of the theory. We find an asymmetry of the non-Abelian plaquette values with respect to the magnetic field. These variables are related to the gluonic part of the energy density of the theory. Thus we expect an influence of the magnetic field also on the equation of state. It would be interesting to conduct a study dedicated to this effect.

ACKNOWLEDGMENTS

E.-M. I. and M. M.-P. thank Mikhail Polikarpov, who was the first to draw their attention to the importance of studying the behavior of non-Abelian gauge fields under the influence of external electromagnetic fields. We thank Edwin Laermann for providing us with the HMC code. A. S. gratefully acknowledges extensive help by Florian Burger in improving and translating the code to the parallel programming and computing platform CUDA. We acknowledge useful discussions with Maria-Paola Lombardo, Falk Bruckmann, Rajiv Gavai, and Sourendu Gupta.

[1] C. DeTar, in Proceedings of the Kyoto Workshop on Thermal Quantum Field Theory and Its Application, 2010, Soryushiron Kenkyu (Study of Particle Theory) (to be published).
[2] T. Vachaspati, Phys. Lett. B **265**, 258 (1991).
[3] D. E. Kharzeev, L. D. McLerran, and H. J. Warringa, Nucl. Phys. **A803**, 227 (2008).
[4] V. Skokov, A. Illarionov, and V. Toneev, Int. J. Mod. Phys. A **24**, 5925 (2009).
[5] S. A. Voloshin (STAR Collaboration), Indian J. Phys. B **85**, 1103 (2011).
[6] B. Abelev *et al.* (STAR Collaboration), Phys. Rev. Lett. **103**, 251601 (2009).
[7] I. Selyuzhenkov (ALICE Collaboration), arXiv:1111.1875.
[8] F. Wang, Phys. Rev. C **81**, 064902 (2010).
[9] B. Müller and A. Schäfer, Phys. Rev. C **82**, 057902 (2010).
[10] V. Voronyuk, V. Toneev, W. Cassing, E. Bratkovskaya, V. Konchakovski, and S. Voloshin, Phys. Rev. C **83**, 054911 (2011).
[11] S. P. Klevansky and R. H. Lemmer, Phys. Rev. D **39**, 3478 (1989).
[12] D. Ebert, K. G. Klimenko, M. A. Vdovichenko, and A. S. Vshivtsev, Phys. Rev. D **61**, 025005 (1999).
[13] A. Zayakin, J. High Energy Phys. 07 (2008) 116.
[14] I. Shushpanov and A. Smilga, Phys. Lett. B **402**, 351 (1997).
[15] J. Schwinger, Phys. Rev. **82**, 664 (1951).
[16] K. Klimenko, Theor. Math. Phys. **90**, 1 (1992).
[17] C. Johnson and A. Kundu, J. High Energy Phys. 12 (2008) 053.
[18] N. O. Agasian, Phys. At. Nucl. **64**, 554 (2001).
[19] N. Agasian and S. Fedorov, Phys. Lett. B **663**, 445 (2008).
[20] A. J. Mizher, M. N. Chernodub, and E. S. Fraga, Phys. Rev. D **82**, 105016 (2010).
[21] P. Cea, L. Cosmai, and M. D'Elia, J. High Energy Phys. 12 (2007) 097.
[22] P. V. Buividovich, M. N. Chernodub, E. V. Luschevskaya, and M. I. Polikarpov, Phys. Lett. B **682**, 484 (2010).
[23] P. V. Buividovich, M. N. Chernodub, E. V. Luschevskaya, and M. I. Polikarpov, Nucl. Phys. **B826**, 313 (2010).
[24] P. V. Buividovich, M. N. Chernodub, E. V. Luschevskaya, and M. I. Polikarpov, Phys. Rev. D **80**, 054503 (2009).
[25] P. V. Buividovich and M. I. Polikarpov, Phys. Rev. D **83**, 094508 (2011).
[26] V. Braguta, P. Buividovich, T. Kalaydzhyan, S. Kuznetsov, and M. Polikarpov, Proc. Sci., LATTICE2010 (2010) 190 [arXiv:1011.3795].
[27] M. D'Elia, S. Mukherjee, and F. Sanfilippo, Phys. Rev. D **82**, 051501 (2010).
[28] M. D'Elia and F. Negro, Phys. Rev. D **83**, 114028 (2011).
[29] G. Bali, F. Bruckmann, G. Endrodi, Z. Fodor, S. Katz, S. Krieg, A. Schäfer, and K. K. Szabó, J. High Energy Phys. 02 (2012) 044.
[30] M. Al-Hashimi and U.-J. Wiese, Ann. Phys. (N.Y.) **324**, 343 (2009).
[31] T. A. DeGrand and D. Toussaint, Phys. Rev. D **22**, 2478 (1980).
[32] E. Laermann, F. Langhammer, I. Schmitt, and P. Zerwas, Phys. Lett. **173B**, 443 (1986).
[33] A. Hasenfratz and F. Knechtli, Phys. Rev. D **64**, 034504 (2001).
[34] V. G. Bornyakov, E.-M. Ilgenfritz, and M. Müller-Preussker, Phys. Rev. D **72**, 054511 (2005).
[35] M. Albanese *et al.* (APE), Phys. Lett. B **192**, 163 (1987).
[36] K. Schilling and G. Bali, Int. J. Mod. Phys. C **4**, 1167 (1993).
[37] R. Sommer, Nucl. Phys. **B411**, 839 (1994).
[38] A. Bazavov, T. Bhattacharya, M. Cheng, C. DeTar, H. Ding *et al.*, Phys. Rev. D **85**, 054503 (2012).
[39] R. D. Pisarski and F. Wilczek, Phys. Rev. D **29**, 338 (1984).
[40] D. Wallace and R. Zia, Phys. Rev. B **12**, 5340 (1975).
[41] P. Hasenfratz and H. Leutwyler, Nucl. Phys. **B343**, 241 (1990).
[42] A. Smilga and J. Stern, Phys. Lett. B **318**, 531 (1993).
[43] R. V. Gavai, S. Gupta, and S. Mukherjee, Pramana **71**, 487 (2008).